JOURNAL OF MATERIALS SCIENCE 28 (1993) 1673–1684

Ceramic joining

Part I *Partial transient liquid–phase bonding of alumina via Cu/Pt interlayers*

M. L. SHALZ, B. J. DALGLEISH, A. P. TOMSIA, A. M. GLAESER
Center for Advanced Materials, Lawrence Berkeley Laboratory, and Department of Materials Science and Mineral Engineering, University of California, Berkeley, CA 94720, USA

A method of ceramic–ceramic joining that exploits a thin layer of a transient liquid phase to join alumina to alumina has been developed, and the results of its application to joining alumina are reported. Through the use of microdesigned multilayer Cu/Pt interlayers, transient liquid-phase joining has been achieved at 1150 °C, yielding an interlayer that is platinum-rich at temperatures substantially lower than those required for solid-state diffusion bonding with pure platinum interlayers. Flexure tests indicate that ceramic/metal interface strengths exceeding those of the ceramic can be achieved. Post-bonding anneals of 10 h duration in air and gettered argon at 1000 °C had discernibly different effects on room-temperature joint strength. The microstructure and chemistry of fracture surfaces were examined using SEM and EDS in an effort to identify the nature of strength-limiting flaws in both as-bonded and post-bonding annealed specimens. Topics requiring further study are identified. Opportunities for extensions of the method to other systems are discussed.

1. Introduction

Fundamental studies of, and innovative approaches to ceramic processing have provided the basis for fabricating ceramics and ceramic–ceramic composites with improved microstructures, properties, and performance. Fundamental studies of ceramic–metal interfaces are providing the scientific basis for processing ceramic–metal composites with improved microstructures, properties, and performance. Currently, there is renewed interest in the processing and properties of refractory aluminides and intermetallics.

These advanced ceramics, ceramic–metal composites, and intermetallics are destined to become the building blocks for complex monomaterial or multimaterial structures with improved or novel properties and function. The fabrication of large complex structures consisting entirely of ceramics will most likely require the joining of smaller components. More complex structures may be designed in which combinations of materials are used to produce an intentional "functional" gradient in a material property. Alternatively, if different regions of a larger structure see vastly differing service conditions, a wide range of materials with varying properties may be used in different regions of the assembly. Joining smaller components to one another will be an essential aspect of fabricating such new structures as well. As a result, fundamental studies of, and innovative approaches to joining these materials to themselves and to one another are required to provide the scientific basis for processing these new structures.

This paper is the first in a series of reports focusing on the application of non-conventional approaches to ceramic–ceramic and ceramic–metal joining. The methods that are being explored use microdesigned multilayer interlayers that incorporate some of the advantages of conventional liquid-state and solid-state joining methods. When the methods are applied to joining ceramics to themselves via refractory metal interlayers, ceramic–metal joints with reduced thermal expansion mismatch and capable of use at elevated temperature can be produced at substantially lower temperatures than those required for conventional joining approaches.

2. Background

Many researchers believe that solid-state diffusion bonding and liquid-based reactive metal brazing are the joining approaches that are most likely to succeed in producing strong joints for demanding high-stress, high-temperature applications. Advocates of diffusion bonding point to the flexibility of the approach, the potential for maintaining dimensional tolerances, and the ability to produce refractory joints as key advantages. Advocates of brazing cite the greater flexibility in joint configuration, less stringent surface preparation requirements, freedom from the need to apply a load that may distort components, and suitability of the method for mass production as among the relative advantages of a brazing approach. Both methods can produce strong joints.

0022–2461

Recently, an interdiffusing multilayer metal interlayer (IMMI) method was developed as an alternative to conventional solid-state diffusion bonding [1]. The process reduces the temperature requirements for forming a strong bond substantially, while retaining the other advantages of diffusion bonding. Studies exploring the use of multilayer Ni/Nb/Ni and Nb/Ni/Nb foils for joining silicon nitride, have demonstrated that strong joints can be produced at significantly lower temperatures than when niobium or nickel foils are used alone. However, the basis for this enhanced bond formation is not fully understood.

A method of joining that would *combine* the best features of diffusion bonding and brazing would be even more desirable. Transient liquid phase (TLP™) bonding provides the most complete merger of benefits. TLP brazing has been applied commercially to the joining of nickel-base superalloys, and has yielded refractory bonds with a strength equivalent to that of the base materials that were joined [2].

The application of TLP bonding to ceramics is limited. Loehman pioneered the use of oxynitride glasses for TLP bonding of silicon nitride ceramics [3]. Subsequent work has examined the role of processing conditions, glass and silicon nitride chemistry, and environmental exposure on the properties and interfacial microstructures of oxynitride glass-bonded silicon nitride [4–7].

In conventional TLP bonding the entire interlayer is molten, and dissolution of the adjoining materials, interdiffusion, and possibly the nucleation and growth of new phases transform the interlayer into a more refractory material at the bonding temperature. Recent independent efforts by Iino [8] and by Glaeser [9] have focused on the development of multilayer *metal* interlayers in which only a *portion* of the interlayer becomes molten. This variation on TLP bonding has been coined *partial* transient liquid phase (PTLP) brazing. The method retains the advantages of TLP bonding, and provides new flexibility in defining the properties of the interlayer and reducing the required bonding temperature. In principle, interlayers can be tailored to the needs of a broad range of material combinations and applications.

3. PTLP bonding

In conventional diffusion bonding, a chemically homogeneous interlayer is used. In reactive metal brazing, layers of titanium or other reactive metals can be deposited directly on the ceramic or can be included in a multilayer foil that homogenizes and melts completely during brazing. Both the IMMI and PTLP bonding methods rely on an inhomogeneous interlayer. For PTLP bonding, a thin film of a low melting point metal or alloy is deposited onto a much thicker foil of a more refractory metal or alloy as illustrated schematically in Fig. 1. Ideally, the refractory metal core can be selected on the basis of its temperature capabilities, thermal expansion coefficient, oxidation and corrosion resistance, or a combination of these and other characteristics. The choice of the low melting point component plays a major role in dictating the processing temperature requirements, with the phase diagram and alloy property information serving to guide the selection of the most appropriate TLP former for a given application.

There are numerous potential mechanisms for "consuming" the low melting point constituent. One approach is to select the two metals or alloys so that the more refractory metal incorporates the less refractory component, and produces a suitably refractory alloy. When such a system is used for PTLP bonding, some of the best features of solid-state and liquid-based joining methods are combined. The low melting point thin film mimics brazing, and relaxes constraints imposed on surface preparation. By design, only a small amount of liquid is formed, and it is formed only where it is needed. Diffusion of the less refractory metal into the refractory host can lead to the disappearance of the liquid at the bonding temperature. If necessary, pressureless annealing or post-bonding hot isostatic pressing at higher temperatures can be used to further homogenize the composition by interdiffusion and to eliminate or reduce the severity of residual interfacial defects.

In conventional brazing, the melting point of the brazing alloy must exceed the intended use temperature; for high-temperature applications, this implies even higher temperature joining. Using a TLP, the

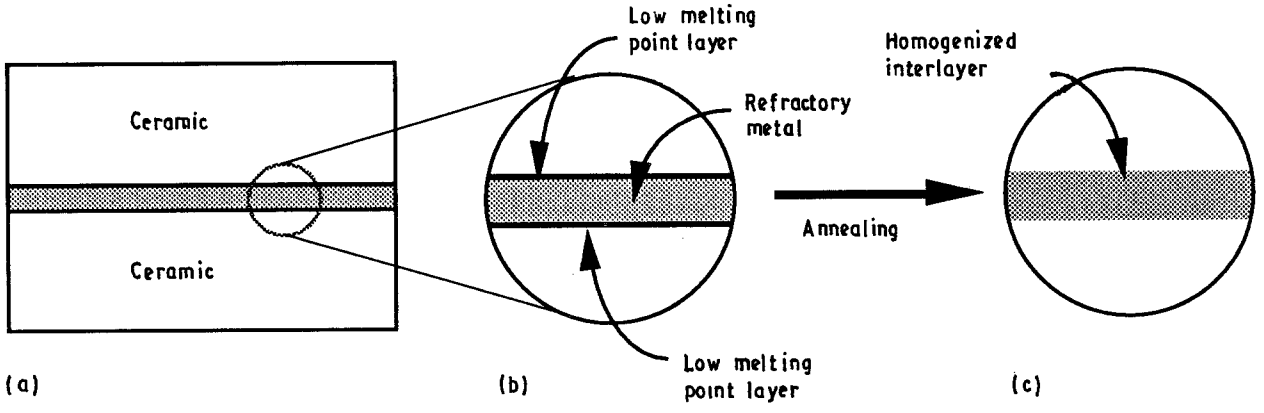

Figure 1 Schematic illustration of (a) ceramic/interlayer/ceramic assembly, (b) detail of microdesigned interlayer prior to heating, and (c) uniform interlayer after partial transient liquid phase bonding or solid-state bonding (and possibly additional heat treatment).

potential exists for forming the joint at low temperature, and for processing at temperatures *less* than or equal to the ultimate use temperature. This minimizes degradation of the ceramic during bonding, and in cases where ceramics are bonded to temperature-sensitive structural metals, avoids overaging of the metal constituent. When more reactive ceramics such as silicon nitride are to be joined, the reduced bonding temperatures may be useful in avoiding detrimental chemical reactions with the metal. The high melting point metal dominates the thermal characteristics of the ultimately uniform interlayer, and can be selected to match the thermal expansion characteristics of the ceramic in ceramic–ceramic joining or to provide an interlayer with intermediate expansion characteristics in ceramic–metal joining. This combination allows the component to be used at high temperature and minimizes thermal expansion mismatch and associated fatigue and failure in thermally cycled assemblies.

Perhaps the simplest implementation of PTLP bonding occurs when the two components of the interlayer exhibit complete mutual solid solubility. Fig. 2 illustrates schematically a simple lens phase diagram for an A–B system. The interlayers are designed such that the ultimate interlayer composition is rich in the more refractory component, as indicated by the shaded region at the B-rich end of the diagram. Conventional brazing and diffusion bonding would require processing temperatures exceeding or approaching the melting point of the refractory interlayer, as indicated by points 1 and 2, respectively. The processing temperatures for the PTLP and IMMI approaches are linked to the melting point of the less refractory component, and are indicated schematically by points 3 and 4, respectively. The homogenized interlayer will have a composition indicated by points 3′ and 4′. Because the melting points of A and B can differ substantially, the potential for reduced processing temperatures is evident.

The Cu–Pt binary system provides a convenient basis for testing the applicability of PTLP bonding to joining alumina to alumina. Platinum is an attractive choice for the metal core for several reasons. Platinum is relatively refractory, melting at 1769 °C, and oxidation and corrosion resistant. Like niobium, platinum matches the thermal expansion of alumina closely; thermal expansion mismatch stresses should be small. Several prior studies of diffusion bonding of alumina via platinum interlayers have been conducted

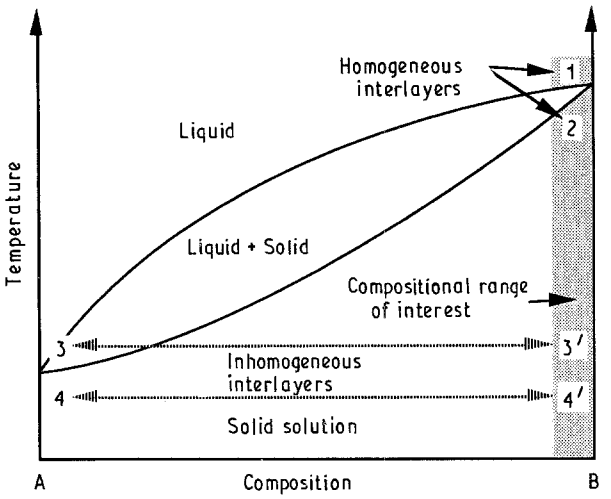

Figure 2 Schematic illustration of bonding conditions relative to phase fields in a simple lens phase diagram. The shaded region indicates the desired average compositions. Condition 1 corresponds to brazing conditions for a homogeneous alloy. Condition 2 corresponds to diffusion bonding conditions that would be required for the homogeneous interlayer. Condition 3′ shows the average composition and brazing temperature for PTLP bonding. The point labelled 3 gives the expected composition of the liquid in contact with the ceramic during joining. Condition 4′ shows the average composition of a multilayer interlayer and the bonding temperature for the IMMI method. The point labelled 4 represents a possible composition of the A-rich alloy in contact with the ceramic during the initial stages of bonding.

[10–15]; a summary of processing conditions in prior Pt–Al_2O_3 bonding studies is provided in Table I. The "strength" of joints has been evaluated in several studies [10–13, 15]. In some instances, failure occurred in the ceramic [12, 15], indicating that platinum–alumina interfaces with a strength exceeding that of the alumina used can be fabricated. Measurements of strength versus temperature indicate that ≈75% of the room-temperature strength can be retained to temperatures up to 1200 °C [11, 12]. Copper is an attractive choice for the TLP former because of its relatively lower melting point (1083 °C), ease of deposition, and because considerable research on Cu–Al_2O_3 diffusion bonding [10, 13, 14, 16–19] and fracture of Cu/Al_2O_3 interfaces [10, 13, 15, 19–23] has been performed. The phase diagram for the Cu–Pt system is also attractive [24]. At temperatures above the melting point of copper, a copper-rich liquid is in equilibrium with a Cu–Pt solid solution, and no brittle Cu–Pt phases form. At temperatures between

TABLE I Reported Pt/Al_2O_3 bonding conditions

Reference	Temperature (°C)	Pressure (MPa)	Time (h)	Maximum strength (MPa)
	1100	0.8		≈60
Allen and	↓	↓	4	↓
Borbidge [12]	1650	0.8		≈225 (four-point bend)
Dalgleish [15]	1450	≈1	2	≈260 (four-point bend)
Klomp [13]	1550	0.03–10	0.33	≈200-250 (four-point bend)

≈816 and 1085 °C, copper and platinum exhibit complete mutual solubility and form a random substitutional alloy. (Cu_3Pt and CuPt, can form at temperatures below ≈735 and ≈816 °C, respectively, and the potential for forming other more platinum-rich intermetallic phases has been indicated [24]. Formation of these brittle phases during cooling prior to sufficient homogenization was a concern.)

4. Experimental procedure

4.1. Materials

The alumina used was 99.5% pure, ≳98% dense, and had a bimodal grain size distribution (Coors, Golden, CO). The material was machined into 19.5 × 20.0 × 22.5 mm^3 blocks. Substrates were hand polished using 30 μm diamond paste on glass, then 15 μm diamond paste on nylon cloth, and finally with 6 μm diamond paste on nylon. The 30 μm polish was aggressive, and although it flattened the bonding surface, it also caused some grain pull-out; these flaws were not removed completely by subsequent polishing. Following polishing, samples were cleaned ultrasonically in isopropyl alcohol for 30 min, and then blown dry with a heat gun. Cleaned substrates were placed in a high-purity alumina crucible, covered, and then annealed in air at 1000 °C for 14 h with the bonding surface exposed to the crucible atmosphere in an effort to remove completely residual organic surface contaminants.

The platinum foil used was 99.95% pure. Pieces 20 mm × 23 mm were cut from a larger 127 μm thick sheet. The foil pieces were cleaned ultrasonically in isopropyl alcohol for several hours. The foil was occasionally turned over in the alcohol during this period. The foil was rinsed in nanopure distilled water (resistivity 18.3 MΩ cm), dried with a heat gun, and then stored in a wafer dish (used in microelectronics processing) until needed.

4.2. Copper coating

Thin layers of copper were deposited on to the alumina by evaporation of a commercial copper wire. (Consolidated Companies Wire and Associated, Chicago, IL). The wire was cut into segments which were then soaked in 2-propanol, rinsed in distilled H_2O, bright-dipped in a 5:1 HNO_3:H_2O solution, rinsed in a second dish of distilled H_2O, soaked in a second dish of 2-propanol, and finally rinsed in nanopure H_2O. The copper wire segments were then placed in the high-purity tungsten baskets of the evaporator for premelting. Premelting was conducted under a vacuum of $\approx 2\text{–}9 \times 10^{-6}$ torr (1 torr = 133.322 Pa). Subsequently, the polished alumina blocks were placed into the evaporator, and copper coated. The chamber pressure was initially at $\approx 3 \times 10^{-6}$ torr, and fluctuated between 7 and 10×10^{-6} torr during deposition.

The copper thickness was measured using two methods. The first relied on a measurement of the mass of a glass cover slip before and after coating. This yielded an estimate of 2.7 mg cm^{-2} for the coating mass, which translates to an average coating thickness of the order of 3.0 μm. The coating thickness was also measured directly by using a profilometer to measure the step height produced where a portion of a glass slide was masked off with the cover slip. Measurements were made at several widely separated points on the glass slide, and thus, at varying distances from the copper source. Coating thickness was not constant, but decreased from ≈3.1 μm to ≈2.7 μm with increasing distance of travel from the copper source. These thicknesses are consistent with an average coating thickness of ≈3 μm, and from this average thickness we deduce an average interlayer composition of ≳94 at % Pt.

4.3. PTLP bonding

Bonding was performed in a vacuum hot press. The block/foil/block assembly was prepared immediately after the completion of coating. Tape was used to hold the assembly together and maintain edge alignment during loading into the graphite hot-pressing die, and was removed after light pressure was applied via rams to the assembly. After an adequate vacuum was achieved, the temperature was ramped to 1150 °C at 4 °C min^{-1}, maintained at 1150 °C for 6 h, and then ramped down to room temperature at 2 °C min^{-1}. During this cycle, the vacuum in the press was in the range of $8\text{–}20 \times 10^{-6}$ torr. A pressure of ≈5.1 MPa was maintained on the assembly during the entire cycle. (This represents the minimum positive load that can be applied to the sample using the hot press available. It is quite possible that a significantly lower load would be sufficient.)

4.4. Beam preparation

The bonded block assembly was mounted onto a glass support plate, and five plates were cut from the bonded block using a diamond wafering saw. The plates were numbered so that any systematic trends in strength or the appearance of the fracture surface could be related to the original position in the block assembly. The plate/support glass assembly was immersed in a detergent solution; this weakened the adhesion between the plates and support glass, facilitating removal of the plates.

One plate surface was polished prior to sectioning of the plates into beams for flexure testing. The nomenclature used to describe the polishing treatments is summarized in Table II. The number following the treatment represents the number of hours for the specific treatment. Plates 1, 3, and 5 were hand polished on plate glass with 30 μm diamond, and then

TABLE II Polishing treatment nomenclature

Treatment	Description
A	Vibratory polish, nylon cloth, 15 μm diamond
B	Hand polish, nylon cloth, 15 μm diamond
C	Hand polish, plate glass, 30 μm diamond
D	Vibratory polish, nylon cloth, 6 μm diamond
E	Automatic polisher, iron lap, 1 μm diamond

polished for more than 100 h with 15 μm diamond on a vibratory polisher, this polishing treatment is designated C2, A > 100. To determine whether an improved surface finish would improve strength, Plate 2 (C2, A > 100, D23) was given an additional 23 h polish with 6 μm diamond, and Plate 4 was polished to a 1 μm finish on an automatic polisher.

Beams of approximately square cross-section (≈3.4 mm × 3.4 mm) were cut from the polished plates with the metal interlayer at the beam centre. The relative positions of the beams in a given plate were indexed. Each beam was assigned an *ij* index where *i* corresponds to plate number, and *j* corresponds to the position relative to the same block assembly face. This procedure was designed to permit a mapping of strength values to position within the original sample. Beam edges were bevelled on the polished face to remove edge flaws that could initiate failure.

4.5. Post-bonding heat treatments

Two plates were given additional heat treatments to determine whether further chemical homogenization of the interlayer and environmental exposure had a discernible effect on the flexure strength. Plate 1 was annealed for 10 h at 1000 °C in high-purity argon passed through a gettering furnace held at 850 °C, and containing titanium-zirconium alloy chips. It was anticipated that this heat treatment would homogenize the interlayer further, and might also modify the oxygen content of the interlayer. Plate 3 was annealed in air for 10 h at 1000 °C. Oxygen diffusion in copper is extremely rapid, and it was anticipated that this annealing treatment might oxidize copper in regions of high copper content, and increase the dissolved oxygen content of the interlayer. The annealed plates were subsequently cut into beams and prepared for flexure testing using the procedure described previously.

4.6. Flexure testing

Beams were tested at room temperature using four-point bending. The inner span was 8 mm. Testing was done with a displacement rate of 0.05 mm min^{-1}. Stress–strain curves showed no evidence of plastic deformation during testing. Strengths were calculated from the load at failure using standard relationships derived for monolithic elastic materials, i.e., no correction for effects of mixed mode loading arising from modulus misfit was attempted. Prior work had determined that four-point bend strengths of (unbonded) alumina beams prepared from the same source material and tested under the same conditions are of the order of 290 MPa.

4.7. SEM/EDS

Pieces that were trimmed from the edge of the bonded blocks to remove offsets created by slight shifting during loading and bonding were polished and subsequently examined using energy dispersive spectroscopy (EDS) to evaluate the extent of diffusion of copper into platinum during the complete bonding cycle. Line scans were conducted perpendicular to the interface. The beam size is typically of the order of 1 μm, and a typical detection limit is ≲1 at %, and thus, we anticipated that this method might provide information on the extent of homogenization achieved during the bonding cycle. A microprobe scan perpendicular to the interlayer was also conducted as a cross-check on the EDS results. At least two stable intermetallics, Cu_3Pt and CuPt, can form at lower temperatures, and thus, the formation of brittle intermetallics near the interlayer/alumina interface was a concern.

Failure often occurred along the ceramic–metal interface, but at widely varying stress levels. The two halves of the fracture surface were mounted adjacent to one another so that equivalent locations on the metal and ceramic side of the fracture surface were in mirror symmetry positions. Flaws and microstructures at matching positions on the two surfaces could thus be identified readily, and were examined using scanning electron microscopy (SEM) in an effort to identify the failure-initiating flaws. The chemistry of fracture surfaces was also assessed to determine whether the different strengths reflected chemically different fracture paths.

5. Results and discussion

5.1. As-processed

5.1.1. Fracture strength

Beams from Plates 2, 4, and 5 were tested to determine the as-processed failure strength, and to assess the effect of tensile surface preparation on failure strength. The quality of the surface finish increased in the order 5 → 2 → 4. Thus, if polishing-induced flaws were determining the strength, one might anticipate that strengths would increase in the same order. The plate/beam strength summary is presented in Table III. There is no obvious trend in the strength values with beam surface preparation.

TABLE III As-prepared flexure strengths

Preparation	Plate (MPa)	Beam				Mean (MPa)	S.D.
		1 (MPa)	2 (MPa)	3 (MPa)	4 (MPa)		
C2, A > 100, D23	2	192	168	148	0[a]	127	87
E	4	203	142	198	64	152	65
C2, A > 100	5	61	180	238	157	159	74

[a] Beam failed during handling. Strength was > 0 MPa, but value of 0 was used in computing mean.

The sample that yielded the highest fracture strength within this set of beams (238 MPa) exhibited ceramic failure. (This is somewhat lower than the "typical" strength determined previously for this material.) More generally, the results indicate that it is possible to achieve high joint strength via PTLP bonding at a substantially lower processing temperature than that required for diffusion bonding. Indeed the highest flexure strengths from this initial set of tests approach those of beams of similar geometry cut from an $Al_2O_3/Pt/Al_2O_3$ assembly diffusion bonded at 1450 °C [15].

The scatter in the strength values is considerable. In one instance, $ij = 24$, the sample failed during handling prior to loading. There is an indication that edge beams ($ij = 24, 44, 51$) are more likely to exhibit low strength. A tendency for lower strengths of edge beams has been observed in diffusion-bonded samples [15] which is quite likely due to rounding of the bonding surfaces during polishing [25]. This rounding produces a fall-off in height as one goes from the sample centre to the edges, and thus, may result in relatively large separation distances and poor edge contact when two crowned surfaces are brought into contact. In the present case, substrate surfaces were not polished to the same degree, and thus, it is uncertain whether these low strengths have a similar origin. The flexure data are limited, and certain edge beams exhibit high strength, e.g. for $ij = 21, 41$.

5.1.2. Fractography and chemical analysis

The microstructure and microchemistry of fracture surfaces of selected beams, spanning low to high (61, 157, 203 MPa) fracture strengths, were examined using SEM and EDS. The general characteristics of the fracture surface were of interest because they would provide information on the degree of bonding achieved, the size and size distribution of interfacial flaws, and insights on the wetting characteristics of the copper-rich liquid layer, and possible guidance on improving the processing procedure. It was also of interest to determine whether the wide variability in fracture strength could be correlated with a difference in the degree of bonding achieved, flaw population, or the chemistry of the fracture surface.

Fracture in the three as-processed samples examined was interfacial, and thus, the microstructures on the metal and ceramic sides of the fracture path could be compared. Three distinct regions/features were evident on the metal side of the fracture surface.

In some regions, grain-boundary grooves outline a coarse-grained (> 150 μm) structure, which we believe reflects the grain structure in the metal foil. (These grain-boundary grooves are evident in the lower right hand corner of Fig. 3a, but can be seen more clearly in Fig. 6c.) In addition, a majority of the area on the metal side also contained an imprint of a finer bimodal (< 10 and > 20 μm) grain-size structure that reflects the grain structure in the ceramic, Fig. 3a. Thus, over much of the ceramic–metal interface, good contact was achieved and maintained during bonding.

There were also regions on the metal side within which the ceramic grain-boundary imprints are absent. Regions in which there is no contact could arise as a result of breakup (dewetting) of the continuous copper-rich film during bonding, or due to the presence of cavities and polishing flaws on the ceramic surface. Fig. 3a and b were taken to produce a mirror image. Comparisons of equivalent positions on the metal and ceramic surfaces suggest that these featureless islands on the metal reflect primarily defects in the ceramic bonding surface. The amount of liquid is apparently insufficient to fill these cavities, and thus, the regions are effectively unbonded. In comparing the low strength and high strength sample, the unbonded regions are larger and the total unbonded area appears to be higher in the low-strength sample.

Chemical analysis of the fracture surfaces was also conducted. Semiquantitative EDS analysis of the metal side of both grain-boundary imprinted and featureless areas on both high- and low-strength samples indicated a composition of ≥ 85 at % Pt, ≤ 15 at % Cu. The probe samples a region ≈ 1–2 μm in diameter

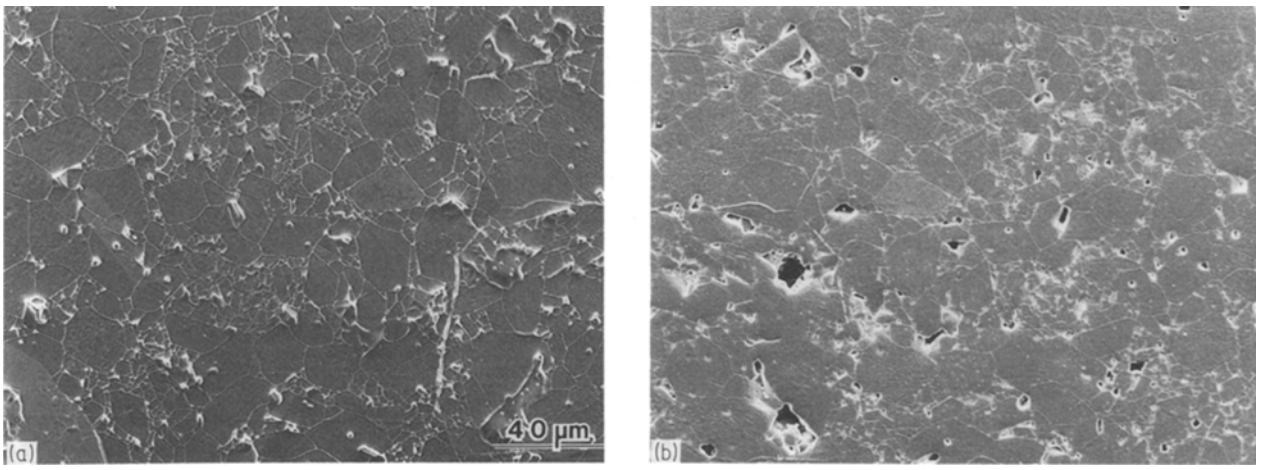

Figure 3 Scanning electron micrographs of (a) the metal side of a fracture surface illustrating the grain-boundary imprints from the ceramic which has a bimodal grain-size distribution, and some evidence of the grain structure of the metal foil, and (b) the corresponding location on the ceramic side. The micrographs are taken and oriented to produce a mirror plane at the junction of the two micrographs. Comparisons of equivalent locations [(x, y) and $(-x, y)$ indicate that the featureless regions on the metal size are the result of surface flaws in the ceramic.

that extends 1–2 μm below the surface. Although the actual surface concentration of copper is presumably higher, the metal fracture surface is platinum-coloured not copper-coloured which also suggests that the surface is not copper-rich. The average near-surface composition lies beyond the platinum-rich limit of the CuPt intermetallic stability region, and suggests that formation of this ordered alloy was avoided. There are indications that an orthorhombic and a cubic $CuPt_3$ phase exist; however, the upper limits of the range of stability are uncertain, and the formation of a thin layer of a platinum-rich intermetallic during cooling to room temperature cannot be precluded. Nonetheless, the EDS results and optical appearance indicate that a significant fraction of the 3 μm thick copper layer diffused into the platinum during the bonding cycle.

EDS profiles were performed on cross sections cut perpendicular to the plane of the interlayer. To generate the profile using EDS, the composition in a small region was determined, the beam position was moved by ≈2 μm, the composition analysed, and the process was repeated until the entire interlayer had been traversed. The results, shown in Fig. 4, indicate a maximum copper concentration of the order of ≈6–9 at % near the interlayer/alumina interface, which decays to ≈1at % at the midplane of the interlayer (a depth of ≈65 μm). The "average" copper concentration in the interlayer calculated from the profile is ≈4.2 at %, which is in reasonable agreement with the average value calculated from the relative thicknesses of the copper and platinum layers. X-ray maps also confirm a substantial penetration of copper.

Multiple microprobe scans were also performed on the same samples, and information on the aluminium, oxygen, copper and platinum concentrations was obtained. The scans indicate three general regions: the alumina, a transition region, and the interlayer itself. In the alumina, the Al:O ratio is as expected for Al_2O_3. Within a transition region, ≈5–10 μm thick, aluminium, oxygen, copper and platinum are all present, and the composition shifts from that of Al_2O_3 to that of a Cu–Pt alloy. Once within the interlayer, the aluminium and oxygen contents are very low or below detection limits. The Cu:Pt ratio is initially of the order 1:10 and decreases as the centre of the interlayer is reached, in close agreement with the results obtained by EDS. However, the microprobe scans also indicate that there are some locations where an ≈20 μm thick core region in the interlayer is copper free. The cause of this spatial variability in the degree of copper penetration is not known. As was the case for the EDS scan, the spatially averaged copper contents within the interlayer are also of the order of 4 at %, somewhat lower than the value expected from the initial average film thickness. (It is possible that because the EDS and microprobe samples are taken from the edge of the block specimen that these corresponded to regions farthest from the copper source during deposition, and thus, regions of relatively lower initial copper coating thickness.)

The most obvious and pervasive physical flaws on the ceramic side of the fracture surfaces were large voids in the ceramic, either intrinsic or reflective of the first stage of substrate surface preparation. One other type of defect, a ≈650 μm diameter region that appeared to reflect contamination, was observed in both the high- and low-strength samples, Fig. 5. Possibly, small droplets of diffusion pump oil were deposited on the surface during the pumpdown period prior to copper evaporation and deposition. In any event, these features were near to or on the non-tensile side of the neutral axis, and thus, not a likely failure origin in either sample.

5.2. Heat-treated post bonding

One of the objectives of PTLP bonding is to produce joints that are capable of use at elevated temperature. In the present study, the effect of 10 h anneals at 1000 °C in both air and high-purity low-oxygen content argon on subsequent room-temperature strength was assessed.

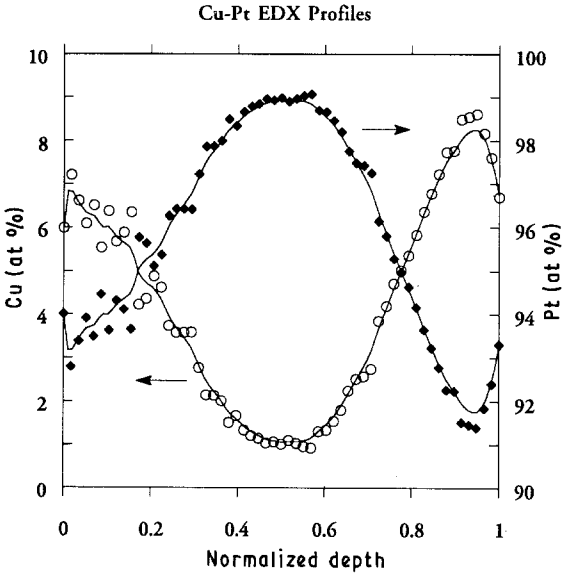

Figure 4 Chemical profile in the interlayer of an as-bonded sample as determined by EDS. Substantial penetration of (○) copper into (◆) platinum is indicated.

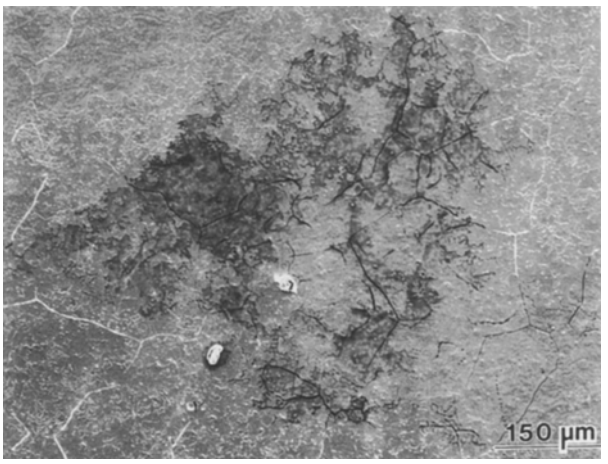

Figure 5 Scanning electron micrograph of a large flaw that appears to reflect contamination on the ceramic surface that evaded cleaning and an air anneal, or more likely, was introduced just prior to copper deposition.

In principle, such post-bonding anneals can have several effects on PTLP-bonded materials. Post-bonding anneals provide a means of homogenizing the interlayer, and reducing thermal expansion gradients. In the present case, this effect should be minimal. Prolonged annealing at elevated temperatures may allow further healing of interfacial defects, and shift the flaw size distribution. Flaw size decreases should increase the flexure strength. High-temperature annealing may reduce the yield stress of the metal, and increase the contribution of plasticity to the work of fracture. This increased toughness should also increase the flexure stress. Anneals in high and low oxygen partial pressure atmospheres can be used to modify the interface chemistry, and this may impact the bonding characteristics at the interface, especially for copper-based PTLPs. Oxygen diffusion in copper at 1000 °C is three orders of magnitude faster than copper self-diffusion [20]. It is possible that the relatively richer in copper Cu–Pt alloy adjacent to the alumina or the ceramic/metal interface itself provides a rapid diffusion path for oxygen into or out of the sample. Recent work by Yoshino indicates that the strength of copper/alumina interfaces is highly sensitive to the oxygen content of the copper [23]. Changes in the oxygen content in the near-interfacial region may then lead to changes in the fracture path by altering the relative energetics of interfacial, metal, and ceramic failure. Changes in the oxygen content may also modify the contact angle between the solid metal and ceramic, and thereby the void perimeter shape. This may modify the stress concentration factor significantly while causing only a minimal change in the void "size". In addition, because only short-range diffusion is required to change the contact angle and pore geometry near the interface, these adjustments should be rapid.

5.2.1. Fracture strength

Annealing in air appeared to have a beneficial effect on the failure characteristics. The minimum strength was 171 MPa, the average was 217 MPa, and the standard deviation (44 MPa) was the lowest of any set. Three of the four beams tested failed at least partially in the ceramic. In contrast, after annealing in argon, all four beams failed along the interface during routine handling prior to testing. Although some stress is applied to the beams during post-bonding cutting and removal from mounting blocks, these stresses must be below ≈ 60 MPa because beams with flexure strengths of this magnitude have survived similar handling steps. Thus, a substantial weakening due to annealing in argon is indicated.

The major difference between the two anneals is the ambient oxygen partial pressure. It seems unlikely that oxygen will accelerate the healing of interfacial defects, particularly at temperatures below the $Cu–Cu_2O$ eutectic temperature, or that argon will impede the healing of interfacial defects. In other words, no substantial effect on transport rates is expected, and it seems reasonable to assume that anneals in air and argon should have a similar effect on the flaw-size population. Neither oxygen nor argon dissolve in platinum to any substantial degree, and thus, effects on the yield strength of platinum, and the plasticity component of the toughness should be similar and minimal. The two most likely causes of the divergent behaviour appear to be changes in the adhesion caused by a change in interfacial chemistry, and changes in the morphology of defects due to chemistry-related changes in contact angle.

Changes in near-interfacial chemistry during annealing in air appear likely in regions that are affected by inward diffusion of oxygen. Thermodynamic data [26–28] indicate that oxidation of copper to Cu_2O in air at 1000 °C is expected when the copper activity exceeds ≈ 0.04. The average mole fraction of copper in the interlayer is $\lesssim 0.06$, but the near-interfacial copper concentration is higher; EDS and microprobe results suggest copper concentrations in the 6–9 at % range. Beraud *et al.* [20] have examined interfacial reactions between copper and alumina during joining. Their results indicate that when a superficial Cu_2O film is present on pure copper, and joining is achieved by means of a copper–copper oxide eutectic liquid, a thin (0.1 μm) layer of a hexagonal binary phase $Cu_2O{\cdot}Al_2O_3$ forms at the metal/alumina interface after only a few minutes at 1070 °C. Thermodynamically, the reaction to form $Cu_2O{\cdot}Al_2O_3$ ($CuAlO_2$) from Cu_2O and Al_2O_3 is associated with a small negative free energy change at 1000 °C [26]. Thus, $CuAlO_2$ is a possible interfacial reaction product during air anneals. (Gadalla and White [26] used data for several reactions involving oxygen that were fitted to an Ellingham form ($\triangle H^\circ - T\triangle S^\circ$) to calculate free energies for several reactions which do not involve the gas phase. The results indicate that reactions to form $CuAlO_2$ from Cu_2O and Al_2O_3, and $CuAl_2O_4$ from CuO and Al_2O_3 have negative free energy changes at 1000 °C. The results also indicate that at temperatures below 1012 °C, the tie-line $CuO–CuAlO_2$ should exist, whereas at temperatures above 1012 °C the tie-line $CuAl_2O_4–Cu_2O$ will exist in the system. However, the authors point out that relatively small errors in the Ellingham slopes could have an appreciable effect on the $\triangle H^\circ$ and $\triangle S^\circ$ values for these reactions. Thus, for anneals in the vicinity of the calculated transition temperature, some uncertainty in the true equilibrium state of the system remains.)

During an anneal in air at 1000 °C, further oxidation of Cu_2O to CuO is expected [26, 27]. The reaction between CuO and Al_2O_3 to form the spinel phase $CuAl_2O_4$ also has a small negative free energy change at 1000 °C [26]. Recent work by Donnet *et al.* [29] has indicated that CuO and $CuAl_2O_4$ precipitates form in copper-implanted polycrystalline Al_2O_3 in response to 1 h anneals at 1000 °C in air [29]. In these experiments, copper is present in the form of metallic precipitates in the alumina, and thus, the copper activity is unity.

In summary, if oxygen diffusion along the alumina/Cu–Pt alloy interface or through the Cu–Pt alloy is sufficiently rapid, internal oxidation of copper and reaction of these oxides with alumina to form binary oxide phases appear to be thermodynamically

TABLE IV Annealed beam flexure strengths

Preparation	Plate	Beam				Mean (MPa)	S.D.
		1 (MPa)	2 (MPa)	3 (MPa)	4 (MPa)		
C2, A > 100, + 10 h in Ar at 1000 °C	1	0[a]	0[a]	0[a]	0[a]	–	–
C2, A > 100 + 10 h in Ar at 1000 °C	3	264	190	171	243	217	44

[a] Beam failed during handling.

possible consequences of air anneals. One would also expect an increase in the dissolved oxygen content in the near-interfacial region relative to that established during bonding. The graphite die is expected to establish an equilibrium oxygen partial pressure of the order of 10^{-33} atm at 1150 °C.

In contrast, anneals in argon were not expected to have a pronounced effect on near-interfacial chemistry. The oxygen partial pressure in the gettered argon when it enters the annealing furnace at 1000 °C is also estimated to be of the order of 10^{-33} atm. Although exact oxygen pressures during bonding and annealing in argon are not known, it seemed unlikely that post-bonding annealing in argon would lead to substantial changes in the dissolved oxygen content, and both the bonding treatment and post-bonding argon anneals would be expected to produce a low dissolved oxygen content in the Cu–Pt alloy.

In this context, the higher strengths of air-annealed samples would be consistent with the view that an increase in the oxygen content, possibly coupled with the formation of a thin reaction layer, promotes the formation of a "stronger" ceramic/metal bond. However, the apparent loss of strength during annealing in argon was puzzling because the oxygen content established during bonding was expected to already be extremely low.

5.2.2. Fractography and chemical analysis

Several considerations motivated fractographic analysis of the air- and argon-annealed samples. Fractographic analysis would allow us to preclude a substantial "statistical" difference in the inherent flaw populations as the basis for the difference in mechanical performance. In addition, through studies of the fracture surfaces, it was hoped that chemically induced changes in interlayer morphology might be detected. The fracture surfaces of one argon-annealed and several air-annealed samples were examined using SEM.

There is no obvious difference in the degree of bonding in the two types of samples; regions in which the imprints of the ceramic grain boundaries are found on the metal are common and occur over similar fractions of the total fracture surface. Fig. 6a–d compare the metal and ceramic sides of the fracture surfaces of air-annealed (a, b) and argon-annealed (c, d) samples, respectively. Thus, we do not believe that the substantial difference in failure stress is a statistical aberration.

At higher magnification some differences in the appearance of the fracture surfaces were observed, generally in the regions of the fracture surface that are near the perimeter of the bonded assembly, and thus, most likely to show the effects of annealing. Selected regions in both air-annealed and argon-annealed specimens had developed a microstructure that was distinct from that characteristic of the remainder of the fracture surface. In addition, the morphologies that developed in these localized regions in air-annealed samples were clearly distinguishable from those that evolved during argon annealing.

Fig. 7 illustrates the structure that evolved during air-annealing. A highly facetted structure has developed on the metal side of the fracture surface (Fig. 7a). Studies of orientation relationships between thin copper films and polycrystalline alumina and sapphire have indicated a preference for the development of a texture in which copper {1 1 1} planes orient themselves parallel to the ceramic surface, but the texture is rotationally isotropic about the plane normal [30]. In the present case, the orientation of the facets appears to be linked to the orientation of the metal grains, with changes in the facet orientation coinciding with the transition from one metal grain to the next. The appearance of the ceramic side on the fracture surface, Fig. 7b, suggests an attack of the ceramic, and is compatible with the expectation that a Cu–Al–O compound, either $Cu_2O{\cdot}Al_2O_3$ or $CuAl_2O_4$, has formed. EDS and X-ray mapping of the facetted structures evident in Fig. 7 were performed, with specific attention given to the detection of aluminium. The EDS results show aluminium present at below 1 at % levels; the microprobe scans across the interlayer showed similar background levels of aluminium. Thus, no compelling chemical information consistent with the development of a Cu–Al–O containing binary oxide was obtained. It is possible that the "reaction layer" is very thin with respect to the thickness of the layer probed, however, the height of the facetted structure in Fig. 7a appears to be of the order of a few tenths of a micrometre, and thus, regardless of whether $Cu_2O{\cdot}Al_2O_3$ or $CuAl_2O_4$ formed, one would expect to detect aluminium. Further work will be required to clarify the nature of the facetted structure that developed.

Fig. 8 illustrates the structure that has evolved during annealing in argon. Dewetting of the ceramic by the metal interlayer is suggested. The morphologies resemble those that develop during the breakdown of

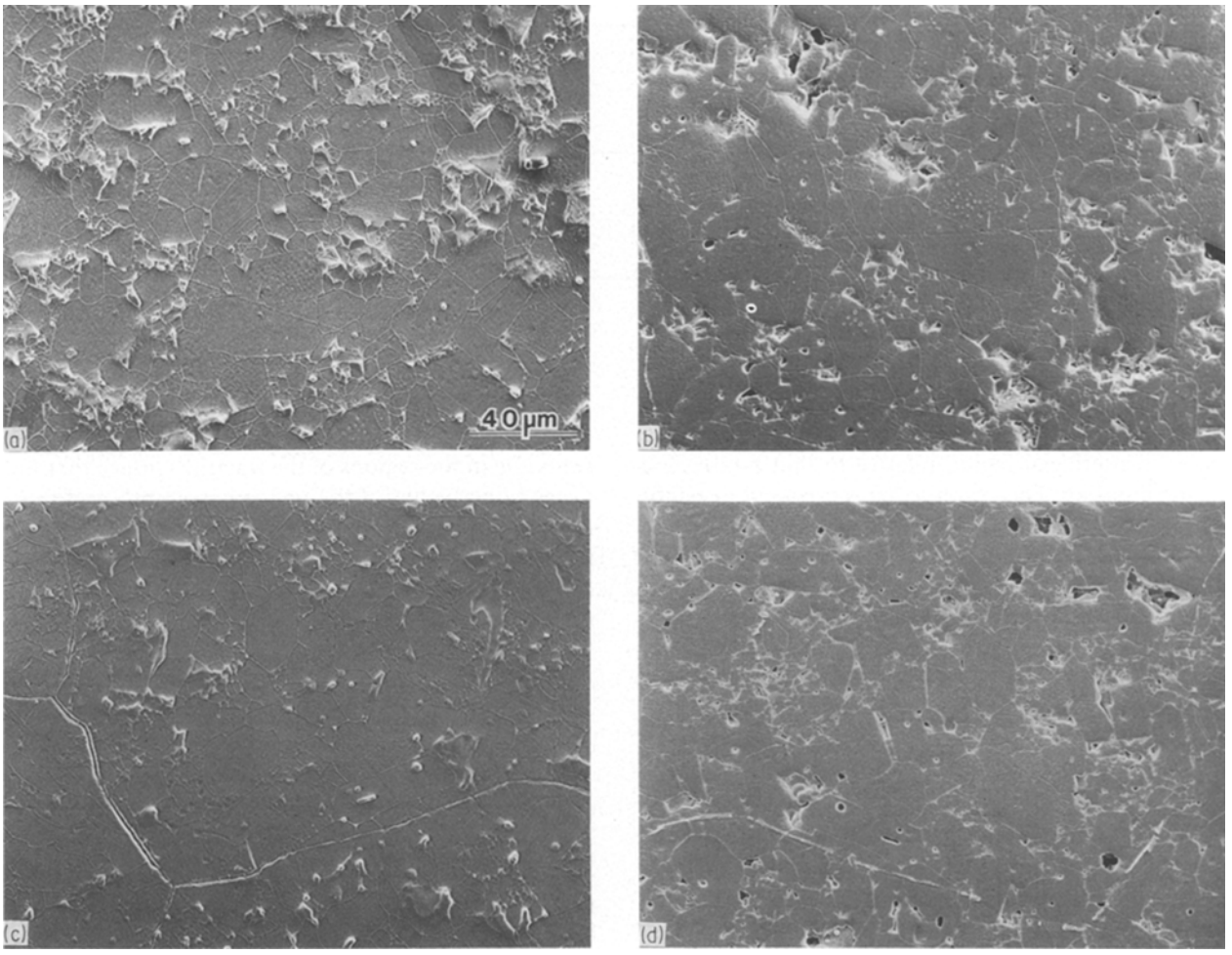

Figure 6 Scanning electron micrographs of the fracture surfaces of an air-annealed (fracture stress 190 MPa) and an argon-annealed (failed during handling) sample: (a) metal side, air anneal, (b) ceramic side, air anneal, (c) metal side, argon anneal, and (d) ceramic side, argon anneal.

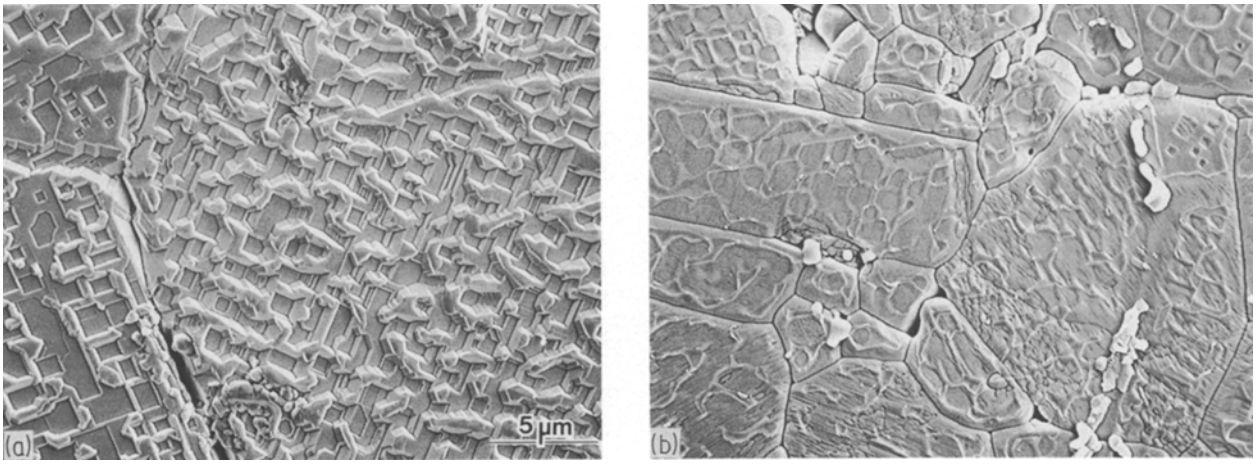

Figure 7 Scanning electron micrographs of (a) the metal side, and (b) the ceramic side of the fracture surface of air-annealed samples. The development of a highly facetted structure is evident. The attack on the ceramic is evident, and suggests that the alumina is a chemical participant in the reaction that forms the facetted structure.

thin metal films on sapphire substrates [30]. Studies of the morphological instabilities of copper thin films on sapphire substrates during annealing under non-oxidizing conditions indicate that such solid-state dewetting can initiate at defects in the film in as little as 10 min at 650 °C.

The present situation is more complex. There is an opportunity for dewetting in the liquid state during bonding at 1150 °C, and the ambient oxygen partial pressure is as low as it is during post-bonding annealing. We expected that the constraint provided by a wettable refractory metal foil would inhibit dewetting

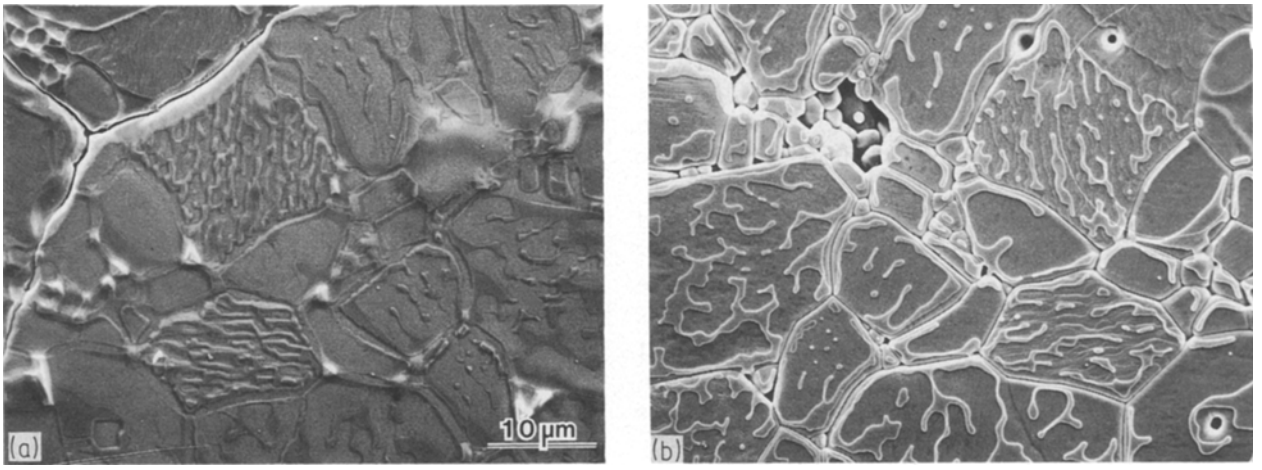

Figure 8 Scanning electron micrographs of (a) the metal side, and (b) the ceramic side of the fracture surface of argon-annealed samples. The structure suggests that solid-state dewetting of Cu–Pt alloy occurred at the interface during annealing, causing a loss of contact and mechanical strength.

during processing, and the fracture surfaces of as-bonded samples support this view. The thin native oxide film that forms on copper at room temperature may also assist in promoting wetting, particularly since the total copper film thickness is only ≈ 3 μm.

The localized solid-state dewetting evident after anneals in argon at 1000 °C may be related to depletion of oxygen (originated from the superficial oxide film on the copper) from the near-interfacial region, and a resulting change in the equilibrium contact angle. Unbonded regions that are open to the ambient atmosphere may provide the analogue to the non-wetting inclusions that serve as the heterogeneous nucleation sites for dewetting of thin films on sapphire [30]. A possible explanation for the difference between the behaviour of as-prepared specimens and the argon-annealed samples may be that during bonding, outward diffusion of oxygen occurs at the block assembly perimeter, whereas during post-bonding annealing the actual tensile surface and the perimeter of flaws that connect to the tensile surface are exposed. This difference in the sample geometry may magnify the importance of the ambient atmosphere during post-bonding anneals of the type conducted in this study. Further and more detailed study of ambient atmosphere effects on the evolution of interfacial microstructure and bond integrity at elevated temperature is needed.

We tentatively conclude that the strength difference observed between air-annealed and argon-annealed specimens reflects a difference in near-interfacial chemistry. In the case of air-annealed samples, an increase in oxygen content in the near-interfacial region relative to that established during bonding is expected, and this may increase adhesion and improve the wetting characteristics of the metal in contact with the alumina. These changes may increase the toughness, and decrease the severity of interfacial flaws. The fracture-surface microstructure suggests formation of Cu–Al–O interfacial reaction products, and these may also have beneficial mechanical consequences. In argon-annealed samples, dewetting of the metal interlayer is indicated, which produces large regions that are poorly bonded and may act as critical flaws. Dewetting may occur preferentially along the perimeter of voids that are open to the external atmosphere, increasing the effective flaw size. An increase in the contact angle resulting from oxygen depletion would also be expected to increase the severity of existing flaws. Several factors may thus contribute to the strength loss in argon-annealed assemblies.

6. Conclusions

The results indicate that high-strength joints between platinum and Al_2O_3 can be produced at lower temperatures than are necessary for diffusion bonding through the use of a thin intervening layer of copper. Fractography results suggest that the scatter in flexure strengths reflects variations in the quality of the bonding surface, and that higher and more uniform strengths should be achievable. The importance of environmental effects on joint strength has been demonstrated. Future work in the Cu–Pt systems will examine the effect of processing conditions (bonding surface preparation, copper thickness, bonding temperature, etc). and post-bonding annealing on strength more thoroughly. A comparison of the fracture toughness and high-temperature mechanical properties of PTLP bonded and diffusion-bonded assemblies would also be of interest.

Although the possibility of forming strong joints was demonstrated with the Cu/Pt system, the method is flexible, and extension of the method to a wide range of systems is possible. Copper and platinum have complete mutual solubility at sufficiently high temperatures. Copper and nickel have similar characteristics, and copper has been used as a transient liquid-phase former to bond Al_2O_3 to nickel using processing conditions similar to those used for Pt/Al_2O_3 bonding. Similarly high strengths have been achieved in as-processed samples [31]. Nicholas [32] has reported that strong Pd/Al_2O_3 can be formed, provided that a void-free interface is achieved. The similarity between the Cu–Ni, Cu–Pt, and Cu–Pd binary phase diagrams suggests that strong Pd/Al_2O_3 bonds can also be produced using copper as the PTLP former. Extension of the method to nickel-rich alloys and

nickel-based superalloys is being explored [33], and extension of the method to include palladium and platinum-rich alloys seems possible. Preliminary experiments have also demonstrated that gold can be used in place of copper [34], and thus, the potential to explore the effects of PTLP chemistry on ultimate bond properties exists.

Although Cu–Ni and Cu–Pt have complete solid solubility at high temperatures, this is not a prerequisite for success. Strong Nb/Al_2O_3 bonds have been produced at 1260 °C using copper interlayers [31]. Nb/Al_2O_3 bonds have also been produced at temperatures as low as 650 °C using a tin-based transient liquid phase [35]; in this case, the PTLP former is most likely consumed by a reaction that leads initially to the formation of a refractory intermetallic. Numerous other mechanisms for consumption of the PTLP former appear possible and are being explored.

Acknowledgements

This paper was written while A. M. Glaeser was on appointment as a Miller Research Professor in the Miller Institute for Basic Research in Science. Helpful discussions and correspondence with R. M. Cannon, Y. Iino, M. Koizumi, M. Nicholas, J. A. Pask and R. Ritchie are acknowledged. Special thanks are due to the Alcoa Foundation for providing the financial resources that allowed the first demonstration of this concept. Additional unrestricted grants from and equipment donations by ARCO, IBM and DuPont contributed to the development of facilities used in this research. This work was supported by the Director's Exploratory Research and Development fund of the Lawrence Berkeley Laboratory under Contract DE-AC03-76SF00098.

References

1. Y. IINO and N. TAGUCHI, *J. Mater. Sci. Lett.* **7** (1988) 981.
2. D. S. DUVALL, W. A. OWCZARSKI and D. F. PAULONIS, *Welding J.* **53** (1974) 203.
3. R. E. LOEHMAN, in "Surfaces and Interfaces in Ceramic and Ceramic–Metal Systems", edited by J. A. Pask and A. G. Evans (Plenum Press, New York, 1981) p.701.
4. R. D. BRITTAIN, S. M. JOHNSON, R. H. LAMOREAUX and D. J. ROWCLIFFE, *J. Amer. Ceram. Soc.* **67** (1984) 522.
5. M. L. MECARTNEY, R. SINCLAIR and R. E. LOEHMAN, *ibid.* **68** (1985) 472.
6. S. M. JOHNSON and D. J. ROWCLIFFE, *ibid.* **68** (1985) 468.
7. S. BAIK and R. RAJ, *ibid.* **70** (1987) C105.
8. Y. IINO, *J. Mater. Sci. Lett.* **10** (1991) 104.
9. A. M. GLAESER, unpublished research (1989).
10. J. KLOMP, in "Science of Ceramics", Vol. 5, edited by C. Brosset and E. Knopp (Swedish Institute for Silicate Research, 1970) p. 501.
11. F. P. BAILEY and W. E. BORBIDGE, in Surfaces and Interfaces in Ceramic and Ceramic–Metal Systems, Materials Research, Vol. 14, edited by J. A. Pask and A. G. Evans (Plenum Press, New York, 1981) p. 525.
12. R. V. ALLEN and W. E. BORBIDGE, *J. Mater. Sci.* **18** (1983) 2835.
13. J. T. KLOMP, in "Electronic Packaging Materials Science", edited by E. A. Giess, K.-N. Tu and D. R. Uhlmann MRS Symposium Proceedings Vol. 40 (Materials Research Society, 1985) p. 381.
14. C. A. M. MULDER and J. T. KLOMP, *J. Phys.* **46** (1985) C4-111.
15. B. J. DALGLEISH, unpublished research (1988).
16. VON W. DAWIHL and E. KLINGLER, *Ber. Deutch. Keram. Gesell.*, **46** (1969) 12.
17. G. HEIDT and G. HEIMKE, *ibid.* **50** (1973) 303.
18. *Idem, J. Mater. Sci* **10** (1975) 887.
19. R. M. CRISPIN and M. G. NICHOLAS, *Ceram. Engng Sci. Proc.* **10** (1989) 1575.
20. C. BERAUD, M. COURBIERE, C. ESNOUF, D. JUVE and D. TREHEUX, *J. Mater. Sci.* **24** (1989) 4545.
21. M. NICHOLAS, R. R. D. FORGAN and D. M. POOLE, *ibid.* **3** (1968) 9.
22. M. WITTMER, C. R. BOER, P. GUDMUNDSON and J. CARLSSON, *J. Amer. Ceram. Soc.* **65** (1982) 149.
23. Y. YOSHINO, *ibid.* **72** (1989) 1322.
24. T. B. MASSALSKI (ed.), "Binary Alloy Phase Diagrams", Vols 1–3 (ASM International, Metals Park, OH, 1990).
25. H. F. FISCHMEISTER, W. MADER, B. GIBBESCH and G. ELSSNER, in "Interfacial Structures, Properties and Design", edited by M. H. Yoo, W. A. T. Clark and C. L. Braint, MRS Symposium Proceedings, Vol. 122 (Materials Research Society, Pittsburgh, PA, 1988) p.529.
26. A. M. M. GADALLA and J. WHITE, *Trans. Brit. Ceram. Soc.* **63** (1964) 39.
27. O. KUBASCHEWSKI and C. B. ALCOCK, "Metallurgical Thermochemistry," 5th Edn (Pergamon Press, Elmsford, NY, 1979).
28. D. R. GASKELL, "Introduction to Metallurgical Thermodynamics", 2nd Edn (McGraw-Hill, New York, 1981).
29. C. DONNET, G. MAREST, N. MONCOFFRE, J. TOUSSET, A. RAHIOUI, C. ESNOUF and M. BRUNEL, *Nucl. Instr. Meth. Phys. Res.* **59/60** Part(II) (1991) 1205.
30. C. M. KENNEFICK and R. RAJ, *Acta Metall.* **37** (1989) 2947.
31. M. L. SHALZ, B. J. DALGLEISH, A. TOMSIA and A. M. GLAESER, unpublished research (1991).
32. M. NICHOLAS, *J. Mater. Sci.* **3** (1968) 571.
33. A. P. TOMSIA, M. L. SHALZ, B. J. DALGLEISH and A. M. GLAESER, unpublished research (1992).
34. M. L. SHALZ and A. M. GLAESER, unpublished research (1991).
35. M. LOCATELLI and A. M. GLAESER, unpublished research (1990).

Received 6 April
and accepted 2 June 1992.